MCB
Journals.ASM.org

Recombinogenic Telomeres in Diploid *Sorex granarius* (Soricidae, Eulipotyphla) Fibroblast Cells

N. S. Zhdanova,[a] I. Draskovic,[b] J. M. Minina,[a] T. V. Karamysheva,[a] C. L. Novo,[b] W.-Y. Liu,[b] R. M. Porreca,[b] A. Gibaud,[b] M. E. Zvereva,[c] D. A. Skvortsov,[c] N. B. Rubtsov,[a] A. Londoño-Vallejo[b]

Institute of Cytology and Genetics, Siberian Branch of the Russian Academy of Sciences, Novosibirsk, Russia[a]; Telomere & Cancer Laboratory, Equipe Labelisée Ligue Nationale contre le Cancer, Institut Curie, Paris, and UPMC University Paris, Paris, France[b]; Moscow State University, Chemical Faculty, Moscow, Russia[c]

The telomere structure in the Iberian shrew *Sorex granarius* is characterized by unique, striking features, with short arms of acrocentric chromosomes carrying extremely long telomeres (up to 300 kb) with interspersed ribosomal DNA (rDNA) repeat blocks. In this work, we investigated the telomere physiology of *S. granarius* fibroblast cells and found that telomere repeats are transcribed on both strands and that there is no telomere-dependent senescence mechanism. Although telomerase activity is detectable throughout cell culture and appears to act on both short and long telomeres, we also discovered that signatures of a recombinogenic activity are omnipresent, including telomere-sister chromatid exchanges, formation of alternative lengthening of telomeres (ALT)-associated PML-like bodies, production of telomere circles, and a high frequency of telomeres carrying marks of a DNA damage response. Our results suggest that recombination participates in the maintenance of the very long telomeres in normal *S. granarius* fibroblasts. We discuss the possible interplay between the interspersed telomere and rDNA repeats in the stabilization of the very long telomeres in this organism.

Telomeres are nucleoprotein structures that protect chromosome ends from degradation and end-to-end fusions (1). Telomeres also play a major role in tumorigenesis, cell senescence, and apoptosis (2). Telomere length, which is an important indicator of telomere function, is the result of the equilibrium between shortening events and lengthening activities (3). To neutralize telomere erosion, which occurs with every cell division, the majority of immortal cells, as well as germ line cells, use telomerase, a dedicated ribonucleoprotein enzyme that is able to add telomere repeats to the 3′ ends of chromosomes (1). However, the majority of human somatic cells express telomerase at very low levels, and as a result, telomeres progressively shorten (2). The sustained loss of telomeric DNA eventually triggers cell senescence, thus limiting the proliferation capacity of somatic cells. This proliferation barrier in humans is deemed to play a fundamental role in tumor suppression (2). It was shown recently that in the case of telomerase-mediated telomere lengthening in the human male germ line and in phytohemagglutinin (PHA)-stimulated leukocytes, an additional mechanism of telomere length control operates, leading to telomere shortening through rapid deletions (telomere trimming) (4). This is a homologous recombination-based excision of the T loop, a structure formed by the folding back of the telomere and invasion of the double-stranded portion by the 3′ telomere overhang (5). The resolution of these T loops results in the production of extrachromosomal T circles (6). The production of T loops is also a characteristic feature of alternative lengthening of telomeres (ALT), a telomere maintenance mechanism based on homologous recombination, found in some telomerase-negative immortal cell lines and primary cancers (7).

Despite the fact that both telomere structure and function are largely conserved from budding yeast to humans, evolutionary approaches to telomere biology in mammalian species have shown that repression of telomerase in somatic tissues as a way to control cell proliferation is not universal. In fact, it appears that most of the species with telomeres whose lengths exceed 25 kb do not use replicative aging (8). What determines this limit and how this feature is related to genome and karyotype evolution among species are not clear.

We showed in previous works that the closely related species *Sorex granarius* and *Sorex araneus*, while exhibiting karyotypes composed of almost identical chromosomal arms, forming either acrocentric or metacentric chromosomes (9), display telomeres with strikingly different architectures (10, 11). For instance, all the chromosome arms found in *S. araneus* carry relatively short telomere lengths (6.8 to 15.2 kb) (12). In contrast, the short arms of *S. granarius* acrocentric chromosomes have extremely long telomeres (average of 213 kb), while telomeres on the long chromosome arms are 3.8 kb long, on average (10). Furthermore, a structural analysis of the very long telomeres in *S. granarius* showed that at least some of them have a discontinuous arrangement, with interspersions of telomeric DNA with ribosomal DNA (rDNA) repeats (11).

In the present work, we investigated the physiology of telomeres in primary *S. granarius* fibroblast cells. We show that *S. granarius* fibroblasts cultured *in vitro* express telomerase and do not display replicative senescence or telomere crisis and that both short and long telomeres appear to remain functional after extended periods of *in vitro* passages. Moreover, along with active telomerase, we found signs of active recombination at telomeres (including a high frequency of telomere-sister chromatid exchanges [T-SCEs], the presence of T circles, and elevated levels of DNA damage response-positive [DDR$^+$] telomeres), suggesting

Received 23 December 2013 **Returned for modification** 15 January 2014
Accepted 28 April 2014
Published ahead of print 19 May 2014
Address correspondence to N. S. Zhdanova, zhdanova@bionet.nsc.ru, or A. Londoño-Vallejo, Arturo.Londono@curie.fr.

doi:10.1128/MCB.01697-13

that recombination mechanisms participate in the maintenance of the very long telomeres of *S. granarius* cells.

MATERIALS AND METHODS

Cells. The primary culture of *S. granarius* fibroblasts was established from pieces of intercostal muscles. Tissue pieces were kindly provided by V. Volobouev. A number of small pieces were placed on the surfaces of 25-ml flasks with a small volume of a culture medium mixture of Igla and F10 media (Biosciences), supplemented with 10% calf embryonic serum (Gibco). Five milliliters of culture medium was carefully added after 1 h. After a few days, fibroblasts formed a confluent monolayer and were passed into a larger flask. Passaging of fibroblasts was then performed every 3 to 4 days. Most experiments were performed with subconfluent cultures containing actively dividing cells.

For chromosome-oriented fluorescence *in situ* hybridization (CO-FISH), cells were cultures in the presence of 10 μM bromodeoxyuridine (BrdU) and 3.3 μM bromodeoxycytosine (BrdC) for 21 h.

For experiments where expression of ICP0* was examined, cells were transfected with the plasmid pAL119::ECFP-ICP0*, encoding an N-terminal enhanced cyan fluorescent protein (ECFP) fusion to the ICP0 ring finger deletion (13, 14). Fifteen million cells were transfected with 40 μg pAL119 by use of Lipofectamine 2000 (Invitrogen) according to the manufacturer's instructions.

For chronic telomerase inhibition, cells were treated with dimethyl sulfoxide (DMSO) or BIBR1532 (10 μM) for 60 days. Cell cultures were maintained at subconfluent levels, and medium containing the solvent or the drug was replaced every 2 days.

Preparation of slides for karyotyping, immunofluorescence (IF), and FISH procedures. For chromosome preparation, cells were treated with 20 ng/ml colcemid (Gibco) for 1 1/2 h prior to hypotonic shock with 0.075 mM (0.56%) KCl for 20 min at 37°C and fixation in a mixture of ethanol (or methanol) and acetic acid (3:1) (13). For routine karyotype analysis, chromosomes were stained with DAPI (4′,6-diamidino-2-phenylindole). FISH and CO-FISH procedures were carried out as described previously (13, 15, 16).

For IF experiments and assays of telomere-induced foci in metaphase spreads (meta-TIF assays), cells or chromosome material was prepared by cytospin centrifugation as described previously (13). Briefly, suspensions of cells or metaphase chromosomes were spread onto slides by centrifugation using a Cytopro 7620 cytocentrifuge (Wescor) at 1,500 rpm for 10 min and then fixed at room temperature for 10 min in freshly prepared 4% (wt/vol) paraformaldehyde in phosphate-buffered saline (PBS) at pH 7.2. After a quick wash in distilled water, cells were permeabilized with 0.1% Triton X-100 in PBS for 10 min at room temperature and used immediately for IF or immuno-FISH experiments.

For the preparation of three-dimensionally (3D) preserved cell nuclei, 15 thousand cells were seeded in 4-well cell culture coverslips (VWR). Preparations were preextracted in 50 mM Tris, pH 8, 150 mM NaCl, 5 mM $MgCl_2$, 300 mM sucrose, and 0.5% Triton X-100 (solution T) for 5 min, fixed in 3% formaldehyde in PBS for 10 min, and permeabilized with solution T for 10 min, all at room temperature.

FISH probes. For telomere FISH, a C-rich peptide nucleic acid (PNA) telomeric probe $(CCCTAA)_3$ labeled with Cy3 (TelPNA-C-rich-Cy3) (Applied Biosystems) was used. In addition, for the CO-FISH experiment, a telomeric G-rich locked nucleic acid (LNA) probe (TelLNA-G-rich-FAM) (custom-made; Exiqon) was used.

rDNA sequences were detected using a 3.2-kb fragment of human 18S rDNA cloned into pHr13 (rDNA-probe) and labeled with biotin-16-dUTP by use of a nick translation kit (Life Technologies). The biotin-rDNA-labeled probe was visualized with avidin conjugated to fluorescein isothiocyanate (FITC; Molecular Probes).

For telomeric repeat-containing RNA (TERRA) detection on chromosomes and interphase nuclei, single-stranded telomere-specific probes recognizing either G-rich or C-rich RNA strands (Telo A probes) were generated as described by Azzalin et al. (17), using PCR and the oligonucleotides $(TTAGGG)_5$ and $(CCCTAA)_5$ (18). The PCR product was labeled by PCR amplification with biotin-16-dUTP (Roche Applied Science) in a deoxynucleoside triphosphate (dNTP) mix either without dCTP (for detection of CCCUAA RNA strands) or without dGTP (for detection of UUAGGG RNA strands). Avidin conjugated to FITC was used for detection (Molecular Probes).

Antibodies. The primary antibodies used were mouse anti-γ-H2AX (613402; Biolegend), with Alexa Fluor 488–goat anti-mouse antibody (R37120; Life Technologies) for detection; rabbit anti-RAP1 antibody (ab4181; Abcam), with Alexa Fluor 488–donkey anti-rabbit antibody (A21206; Life Technologies) for detection; and mouse anti-UBF (sc-13125; Santa Cruz), with Alexa Fluor 488–goat anti-mouse antibody (R37120; Life Technologies) for detection. For the delineation of centromeric regions, a patient serum containing human anti-centromere-protein antibody, also known as CREST serum, was used (15-235-0001; Antibodies Incorporated), with FITC–donkey anti-human antibody (109-097-003; Jackson ImmunoResearch) for detection.

FISH. FISH on metaphase spreads or interphase nuclei, using rDNA and a telomeric PNA probe, was performed as described previously (13, 15, 16). Images were acquired by confocal microscopy (LSM 710; Zeiss).

Quantitative FISH (Q-FISH) and CO-FISH were performed according to established protocols, using strand-specific telomeric PNA (C-rich) and LNA (G-rich) telomeric probes (19).

For Q-FISH analysis, 10 metaphase spreads from both primary (passage 7) and long-term (passage 116) *S. granarius* fibroblast cultures were used for comparative analysis of long and short telomere intensities. All manipulations, including hybridization with the PNA probe, were performed simultaneously for both cultures. Registration of all signals was made in a single photo session with identical acquisition settings. Telomeric signal intensities were quantified using Isis 5 imaging software (MetaSystems). The real intensity of a telomere signal was calculated as the difference between the signal intensity from a telomere region and the mean background signal for three background regions equal in size to a telomere region chosen in proximity to each analyzed telomere. Statistics were performed using the Mann-Whitney U test in Statistica 10.

Meta-TIF assay. The meta-TIF assay for detection of telomere-induced foci (TIF) in metaphase spreads was performed as described previously (13). Briefly, metaphase spreads prepared by centrifugation were fixed with formaldehyde and subjected to immunofluorescence (IF). Slides were washed once with PBS and treated with RNase A (0.1 mg/ml) in ABDIL buffer (50 mM Tris, pH 7.5, 150 mM NaCl, 2% bovine serum albumin [BSA], 0.1% Triton X-100, 0.2% fish gelatin [Sigma]) for 30 min at 37°C in a humidified chamber. After three washes in PBS, slides were incubated with anti-γ-H2AX antibody (1:1,000) followed by the secondary antibody. Antibodies were diluted in ABDIL buffer, all incubation steps were done in a humidified incubator at 37°C for 1 h, and after each incubation with antibodies, slides were washed in PBST (0.1% Tween 20 in PBS) three times for 5 min each. For subsequent FISH experiments, IF slides were fixed with 4% (wt/vol) paraformaldehyde in PBS for 10 min, rinsed in PBS once, and dehydrated in a 70%, 80%, 90%, and 100% ethanol series. FISH with the TelPNA-C-rich probe was performed as described above. Slides were either stained with DAPI (50 ng/ml) diluted in 2× SSC (1× SSC is 0.15 M NaCl plus 0.015 M sodium citrate), air dried, and mounted in Vectashield (H-1000; Vector) or directly mounted in Vectashield containing 0.2 μg/ml DAPI. In certain cases, IF and FISH experiments were performed sequentially (two-step protocol), with separate imaging after immunostaining and FISH (for anti-centromere CREST serum and anti-γH2AX antibodies).

TERRA-FISH. TERRA-FISH on metaphase spreads and on interphase nuclei was carried out as described previously (17). Briefly, cells grown on slides were permeabilized with freshly made CSK buffer [100 mM NaCl, 300 mM sucrose, 3 mM $MgCl_2$, 10 mM piperazine-*N*,*N*′-bis(2-ethanesulfonic acid) (PIPES), pH 7, 0.5% Triton X-100, 1 mM EGTA] containing 10 mM vanadyl ribonucleoside complex (Sigma) for 10 min at 4°C. Slides were rinsed in PBS, fixed for 10 min in freshly made 4% paraformaldehyde

in PBS, and rinsed in 70% ethanol, all at room temperature. Preparations were then dehydrated through an ethanol series (70%, 90%, and 100%; 3 min each at room temperature) and air dried. For the RNase treatment, slides were incubated with RNase A (Sigma) (10 mg/ml) for 1 h at 37°C in a humidified chamber before the application of the probe. Telo A probes (see above) were dissolved in 10 μl deionized formamide, denatured at 74°C for 7 min, and chilled on ice. Ten microliters of hybridization buffer, containing 4× SSC, 4 μg/μl BSA, 20% dextran sulfate, and 20 mM vanadyl ribonucleoside complex, was added to the probe, mixed well, and applied to slides. Hybridization was carried out for 16 h in a humidified chamber at 37°C. After hybridization, slides were washed in 50% formamide–2× SSC, 3 times for 5 min each, and then in 2× SSC buffer, 3 times for 5 min each, at 37°C. Slides were dehydrated through an ethanol series (70%, 90%, and 100%; 2 min each at room temperature), counterstained with DAPI, and mounted in Vectashield.

Image acquisition and analysis. IF and FISH images were acquired using either a confocal microscope (LSM510 Meta; Zeiss) or an Axioplan 2 imaging microscope (Zeiss) equipped with a charge-coupled device (CCD) camera (CoolCube 1; Meta Sistems), a Chroma filter set, and Isis 3 software at the Center for Joint Ownership for Microscopic Analysis SB RAS (ICG SB RAS, Novosibirsk, Russia). For 3D analysis, images were taken with a 3D deconvolution microscope (Leica model DM6000 B or Nikon model Ni80) using MetaMorph software. Final images are composed of arithmetic stacks of 20 to 30 deconvolved images, each with a depth of 0.2 μm.

Northern blot analysis of TERRA. Total RNA was extracted with an RNeasy minikit (Qiagen) according to the manufacturer's instructions. Remaining traces of DNA were digested with DNase I (Qiagen). Ten or 20 μg of total RNA was separated by alkaline electrophoresis in a 1% agarose–1.3% formaldehyde gel and transferred to a Biodyne B positively charged membrane (VWR). Blots were blocked with modified Church buffer (500 mM Na_2HPO_4, 7% SDS, 1 mM EDTA) and hybridized overnight at 42°C in modified Church buffer with a digoxigenin-labeled telomeric C-rich LNA probe (custom-made; Exiqon) to reveal TERRA (G-rich). Blots were then washed twice for 5 min each with 2× SSC–0.1% SDS, washed for 2 min with 0.2× SSC–0.1% SDS, and rinsed in 2× SSC. The C-rich probe was revealed using antidigoxigenin–alkaline phosphatase antibodies and a CDP-Star detection kit (both from Roche) according to the manufacturer's instructions. The blot was then stripped (incubation twice for 15 min each time in 0.5% SDS at 60°C and twice for 15 min each time in 0.2 N NaOH–0.1% SDS at 37°C) and revealed again, using the antidigoxigenin Roche detection protocol, to ascertain the efficiency of stripping. The stripped membrane was hybridized with a telomeric G-rich oligonucleotide probe [$(TTAGGG)_4TTA$] 3′-end labeled with digoxigenin (Roche Applied Science) to detect C-rich RNA transcripts. Hybridization washes and detection steps were performed as described above for the telomeric C-rich LNA probe hybridization.

TRAP. Telomerase activity was revealed according to the regular telomeric repeat amplification protocol (TRAP), as recommended previously (20), or using semiquantitative TRAP (qTRAP), also as described previously (21). Gel density analysis for regular TRAP was performed with Image Quant TL 1D gel analysis software. Total densities of all bands in a line with the minimum profile background subtraction were quantified.

2D gel electrophoresis. For detection of T circles, DNA was purified from *S. granarius* cells by use of phenol. MboI-digested restriction fragments were first separated by size in 0.4% Ultrapure agarose (Invitrogen) in 1× Tris-borate-EDTA (TBE) at ~1 V/cm overnight and then by shape in the second dimension, using 1% agarose in 1× TBE containing 0.1 μg/ml ethidium bromide. Gels were blotted onto Biodyne B positively charged membranes (VWR) and probed with a digoxigenin-labeled telomeric LNA probe (custom-made; Exiqon). Hybridization was carried out overnight at 42°C in modified Church buffer. Hybridization washes were performed in 100 mM Na_2HPO_4 and 2% SDS. The digoxigenin-labeled probe was detected using antidigoxigenin–alkaline phosphatase antibodies and a CDP-Star detection kit (both from Roche) following the manufacturer's instructions.

C-circle detection. For the detection of C circles, cells were collected by trypsinization, resuspended in 300 μl PBS, and lysed with an equal volume of either 2× Hirt buffer (20 mM Tris, pH 7.5, 200 mM NaCl, 20 mM EDTA, 01% SDS) or 2× buffer T (20 mM Tris, pH 7.5, 20 mM NaCl, 20 mM EDTA, 1% sarcosyl). Lysates were treated with RNase A for 1 h at 37°C and with proteinase K at 55°C overnight and then extracted with phenol-chloroform-isoamyl alcohol (Invitrogen) followed by chloroform-isoamyl alcohol (Sigma), using 5 Prime PhaseLock gel (Fischer). DNA was precipitated using 2 volumes of ethanol containing a 1/10 volume of sodium acetate for 1 h at −80°C and then centrifuged at 16,000 × *g* for 30 min at 4°C. Ethanol-washed pellets were dried with a SpeedVac (no heat) and resuspended in 10 mM Tris, pH 7.5, to prevent the acid hydrolysis of DNA. Five micrograms of genomic DNA was digested overnight with HinfI and RsaI (40 U each). In the morning, an additional 10 U of each enzyme was added, and the digestion was continued for another 2 h before precipitation of DNA with ethanol-sodium acetate. For C-circle amplification, 500 ng of digested genomic DNA was incubated with Phi 29 polymerase (Fermentas) in the presence of the buffer provided by the manufacturer and 2 mM (each) dATP, dGTP, and dTTP at 30°C for 12 h. DNA or Phi polymerase was omitted from the reaction mixture as a negative control. In addition, the C-circle amplification was executed in the presence of all 4 nucleotides to facilitate the amplification of circles containing variant telomeric repeats. The reaction was stopped by heating samples to 65°C for 20 min. Samples complemented with 6× loading buffer (300 mM NaOH, 6 mM EDTA, 15% Ficoll 400, 0.25% xylene cyanol FF) were separated in a 0.8% alkaline agarose gel (50 mM NaOH, 1 mM EDTA) for 20 h at 1 V/cm in a cold room. After neutralization in 0.7 M Tris, pH 7.6, 300 mM NaCl, the gel was stained with ethidium bromide for visualization of the molecular weight standard. After depurination in 0.25 M HCl for 10 min and neutralization in an alkaline transfer buffer (0.4 M NaOH, 1.5 M NaCl), the gel was transferred by capillary transfer onto a Biodyne B positively charged membrane (VWR). Products amplified by the rolling circle amplification of C circles were detected by hybridization to a digoxigenin-labeled C-rich telomeric oligonucleotide [$TAA(CCCTAA)_4$]. The signal was revealed using a digoxigenin detection kit (Roche) and the CDP-Star reagent.

RESULTS

The short arms of *Sorex granarius* chromosomes are truly acrocentric. We previously showed that at least some of the long telomeres in *S. granarius* short chromosome arms present a discontinuous primary structure, with interspersions containing large blocks of 18S rDNA repeats (11). To gather information about the functional and structural organization of these short arms, we explored the possibility that functional centromeres are actually positioned close to both the rDNA and telomere sequences. Using ANA-CREST antibodies and two-color FISH, with specific probes against telomeres or 18S rDNA, we showed that centromeres are either adjacent to or overlap signals from both telomeric DNA and rDNA (Fig. 1A). This indicates that unique centromere structures are formed close to the tip of every short arm of acrocentric chromosomes, therefore supporting the notion that *S. granarius* carries true acrocentric chromosomes.

The telomere-associated rDNA loci in *S. granarius* are not always expressed. We previously demonstrated a tight association between the very long telomeres of *S. granarius* and potentially active nucleolar organizing regions (NORs), as suggested by antigen staining (11). Since formation of active nucleoli actually requires the binding of UBF1 (upstream binding factor 1), a transcriptional factor that binds to rDNA promoters, thus favoring the recruitment of RNA polymerase I (Pol I) (22), we wished to de-

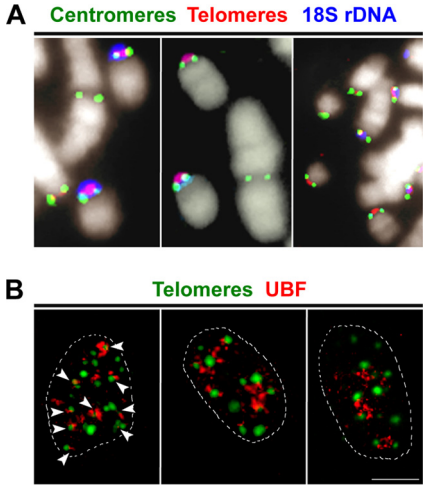

FIG 1 Position of centromeres and nucleolar relationship of acrocentric chromosomes in primary *S. granarius* fibroblasts. (A) Centromere position on *S. granarius* acrocentric chromosomes. A two-step experiment was performed, including immunofluorescence assay with ANA-CREST antibodies to detect centromeric proteins (green) and subsequent two-color FISH with a C-rich telomeric PNA probe (Cy3; red) and an 18S rDNA probe (pseudocolored blue). Chromosomes were counterstained with DAPI (pseudocolored white). Centromeres are generally found adjacent to or overlapping signals from telomeric and rDNA probes. (B) Visualization of transcriptionally active nucleoli in primary *S. granarius* fibroblasts by use of anti-UBF1 antibodies (red). Telomeres were subsequently visualized through PNA FISH (green). In the optical slice at left, arrows indicate close contacts between telomeres and nucleoli. The mean number of nuclear telomere foci (± SEM) was 13.7 ± 2.8 (range, 9 to 26), with 65% ± 2.6% of them being in association with UBF1 signals ($n = 90$ nuclei). Bar, 10 μm.

termine the frequency with which UBF1 is found close to long telomeres in interphase nuclei (Fig. 1B). We found large UBF1 spots, corresponding to active nucleoli, associated with 65% of all telomeric foci visible in the interphase nuclei of primary *S. granarius* fibroblasts. Although part of this less-than-perfect colocalization of large telomeric foci with UBF1 could be explained by the previously described cell cycle-related variation of transcriptional activity of 45S rRNA genes by RNA Pol I (23), it also suggests that not all rDNA clusters associated with telomeres or interspersed with telomere repeats are expressed in *S. granarius*.

***S. granarius* fibroblasts maintain telomere function after prolonged *in vitro* culture.** *S. granarius* cells were isolated from an intercostal muscle biopsy specimen, cultured, and amplified for 10 to 12 passages as primary fibroblasts. We also maintained a long-term cell culture in order to evaluate proliferation capacity and telomere stability. Fibroblasts were able to proliferate for about 2 years, with no signs of growth crisis between early and late passages. In fact, the population doubling times for primary fibroblasts and long-term-culture fibroblasts were not very different (24 ± 2.3 h and 20.9 ± 1.8 h, respectively). Karyotypic analyses did not reveal major chromosomal structural rearrangements in long-term-culture fibroblasts (Fig. 2A). However, we observed aneuploidy in long-term cell cultures, with the appearance of additional acrocentric chromosomes similar in size and banding to the small acrocentric chromosomes of the *S. granarius* karyotype. After 2 years of cell culture, only 4% of fibroblasts contained a normal diploid chromosome set (36 chromosomes), whereas 27% carried one additional chromosome and the majority (69%) carried two additional chromosomes (Fig. 2B). Monosomes were observed at a very low frequency. The mechanisms leading to aneuploidy were not explored here but may be related to partial endoreduplications and/or to nondisjunctions. Similar to those from primary fibroblasts, chromosomes from long-term-culture fibroblasts carried both long and short telomeres, exclusively associated with short and long arms of acrocentric chromosomes, respectively (Fig. 2C). Q-FISH analysis showed that intensities of telomeric signals on short and long arms slightly, although significantly ($P < 0.05$), decreased with prolonged passages (Fig. 2D and Table 1). While long telomeres remained heterogeneous, short telomeres appeared to be distributed more homogeneously at late passages (Fig. 2D). Despite this relatively limited shortening, we did not detect any signs of karyotypic rearrangements that could arise from telomere fusions, which strongly suggests that telomeres remained functional throughout cell growth and, in particular, successfully suppressed all nonhomologous end-joining (NHEJ) repair activities directed against chromosome ends.

***S. granarius* fibroblasts are telomerase positive.** In many species, maintenance of telomere lengths during long-term *in vitro* growth of somatic cells is usually associated with the presence of telomerase, the reverse transcriptase able to elongate telomeres and to counteract replication-related telomere losses. We tested whether telomerase activity was detectable in *S. granarius* primary and long-term-culture fibroblasts. Experiments using both conventional TRAP assay (Fig. 3A and B) and real-time TRAP assay (Fig. 3C) revealed the presence of active telomerase in both primary and long-term-culture fibroblasts. Telomerase activity appeared to be increased slightly in long-term-culture fibroblasts compared to primary fibroblasts (Fig. 3A and B). Although this apparent increase in telomerase activity did not prevent telomere shortening (see above), it may account for the relative homogenization of telomere length distribution at late passages (16).

***S. granarius* fibroblasts display ALT-associated PML-like bodies.** Telomere lengths can be maintained independently of telomerase, through recombination by alternative lengthening of telomeres (ALT) (24). Given that telomeres in *S. granarius* are largely heterogeneous between chromosome arms, which is a characteristic of ALT (25), we looked for the presence of other ALT hallmarks in these cells (7). We first looked for the presence of ALT-associated PML bodies (APBs). In ALT cells exclusively, telomeres form aggregates that associate with PML bodies (26). Such interactions most likely facilitate the telomeric recombination reactions (13). It has been shown before that telomeres in *S. granarius* tend to aggregate in interphase nuclei and that some of these aggregates colocalize with nucleolar markers (27), as also shown here (Fig. 1B). We now tested the possibility that some of these aggregates also contain the PML protein, the major component of PML nuclear bodies (PML NBs). To do this, we used the available antibodies against human PML and SP100, another conserved protein found in these bodies. Unfortunately, none of the tested antibodies revealed specific foci in *S. granarius* fibroblast nuclei.

We therefore tried an alternative approach based on the fact that the ICP0 protein of the human herpes simplex virus can very specifically interact with PML (28). Specifically, a mutated version of the ICP0 protein (ICP0*) is able to bind PML without inducing its degradation, and thus strongly accumulates in PML NBs or in APBs,

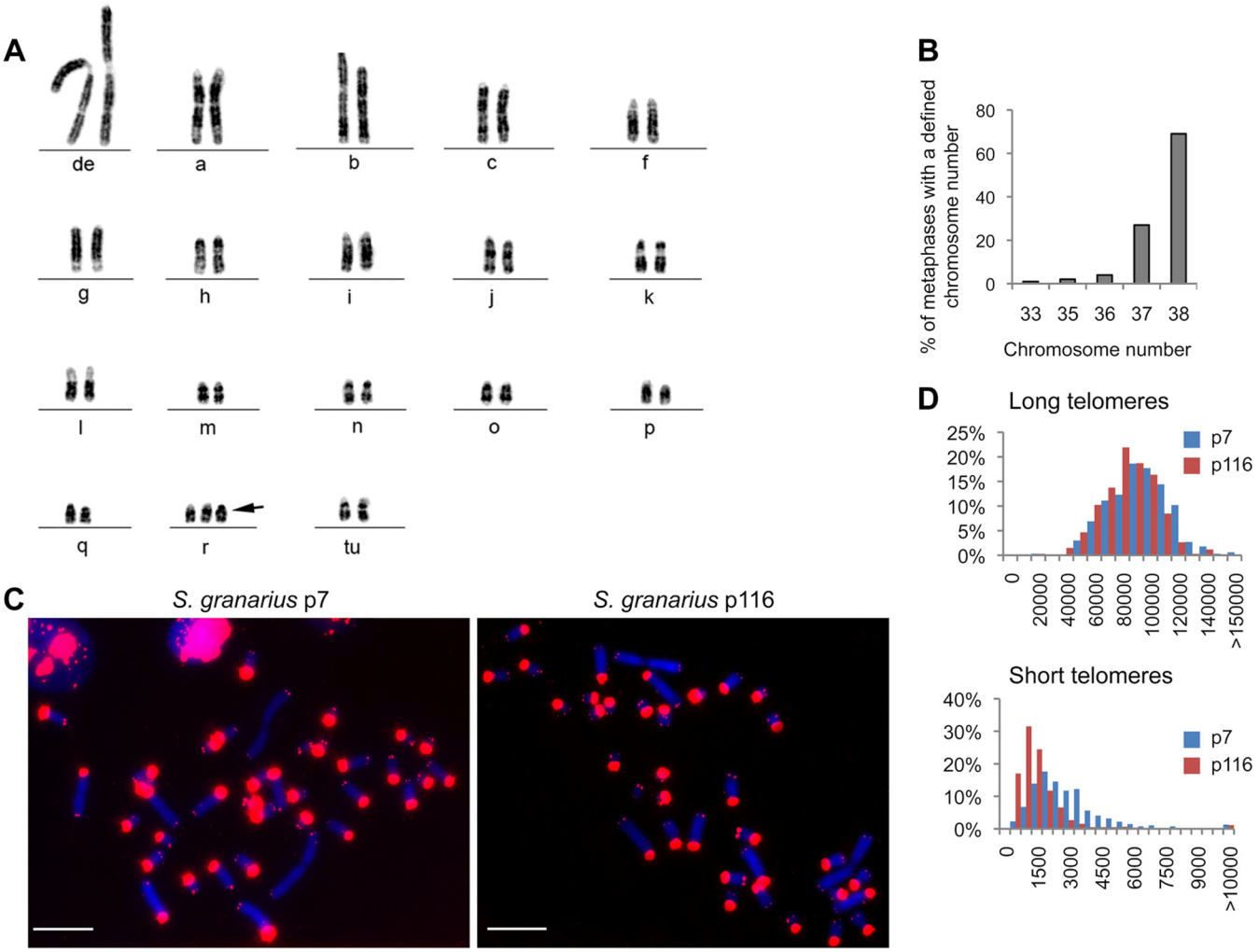

FIG 2 Chromosome stability in long-term-culture *S. granarius* fibroblast cells. (A) Representative karyotype of *S. granarius* fibroblasts in long-term culture (passage 132; approximately 1 1/2 years). The diploid chromosome complement in female *S. granarius* is 36, with 32 acrocentric chromosomes and 4 metacentric chromosomes. Arrow, additional chromosome "r." (B) Chromosome number variation in late-passage fibroblasts (passage 132). Two hundred metaphase spreads were analyzed. (C) Representative images of telomere length analysis by Q-FISH on metaphase chromosomes from primary (passage 7; p7) and long-term (passage 116; p116) fibroblast cultures. The telomeric PNA C-rich probe (Cy3; red) was used, and chromosomes were counterstained with DAPI. The telomere length inequality reported previously for primary fibroblasts (long telomeres on short arms of acrocentric chromosomes versus very short telomeres on all other extremities [10]) was preserved in long-term cultures. Bars, 10 μm. (D) Quantification of Q-FISH telomere intensities for long and short telomeres. See Table 1 for more details.

TABLE 1 Telomere lengths in primary and long-term-culture *S. granarius* fibroblasts[a]

Telomeres and passage	No. of telomeres analyzed	Mean fluorescence intensity ± SEM
Long		
7	333	88,392.5 ± 1,200.7
116	342	81,593.8 ± 2,613.9*
Short		
7	785	2,718.7 ± 69.1
116	794	1,494.3 ± 111.2*

[a] Telomere lengths were measured by Q-FISH after short- and long-term culture of primary *S. granarius* fibroblasts. Limited (but significant) reductions in telomere length were recorded for both long and short telomeres. *, $P < 0.05$ by Mann-Whitney U test.

provoking the enlargement of these bodies to the point that associated structures, such as chromosome ends in the case of APBs, are individualized (13). We reasoned that if ICP0* can target the *S. granarius* PML protein, it will be able to recognize nuclear structures equivalent to PML NBs in this species, thus allowing us to verify whether or not telomeres are associated with these structures. Indeed, when primary *S. granarius* fibroblasts were transfected with a construct expressing a fluorescent version of ICP0*, the protein formed large nuclear foci (between 7 and 24 foci [mean ± standard error of the mean {SEM}, 18 ± 1.94 foci] per transfected nucleus; $n = 220$) (Fig. 4A). The shape and number of these foci are not very different from those of the PML NBs in other species (29), suggesting, albeit not proving, that the structures revealed by ICP0* in *S. granarius* fibroblasts were bona fide PML NBs. Despite this caveat, we decided to test whether ICP0*$^+$ NBs were associated with telomere sequences. As shown in Fig. 4B and C, many strong telomeric foci were in close

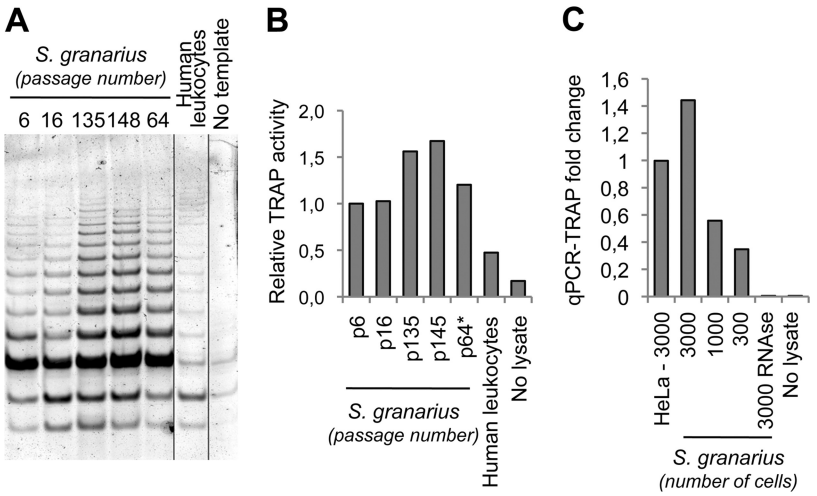

FIG 3 Fibroblasts of *S. granarius* contain active telomerase. (A and B) Conventional TRAP analysis of *S. granarius* fibroblast cells revealed telomerase activity in primary and long-term-culture cells. (A) DNA PAGE gel after conventional TRAP using protein extracts from *S. granarius* fibroblasts at different passages. A protein extract from PHA-stimulated human leukocytes was used as a positive control. (B) Densitometric analysis of conventional TRAP results. (C) A real-time semiquantitative TRAP assay was performed on cell extracts prepared from early-passage *S. granarius* cells (passage 9) and compared to the activity found in an equal number of human HeLa cells. Serial dilutions of *S. granarius* whole-cell extracts (3,000, 1,000, and 300 cell equivalents) resulted in a decreased TRAP activity. Treatment with RNase A and omission of the cell extract served as negative controls.

association with ICP0*$^+$ NBs (12 to 43% of telomeric foci; mean ± SEM, 23% ± 3.1%; $n = 160$). Furthermore, telomeric signals of low intensity were also frequently seen on the periphery of numerous ICP0*$^+$ NBs (Fig. 4B and C).

To further ascertain the association of telomeric structures with ICP0*$^+$ NBs, we tested the presence of shelterin proteins in these bodies. As for PML and SP100, most antibodies directed against human shelterin components failed to show any specific IF

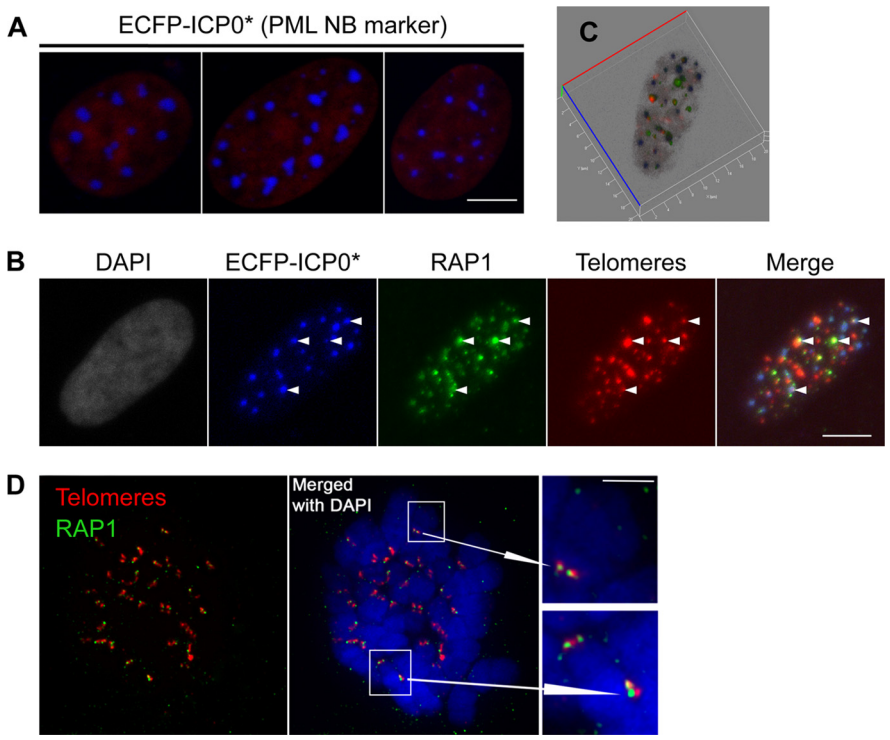

FIG 4 *S. granarius* fibroblasts carry APB-like structures. (A) *S. granarius* primary fibroblasts (passage 7) were transfected with a plasmid expressing an ECFP-ICP0* fusion to reveal putative PML nuclear bodies. The native fluorescence of the ECFP-ICP0* fusion in three transfected nuclei is shown. ICP0* formed 7 to 24 (18 ± 1.94 [mean ± SEM]) large nuclear foci per transfected nucleus ($n = 150$ nuclei). (B) Cells expressing ECFP-ICP0* were costained with antibodies against the human shelterin protein RAP1 (green) and with a telomeric C-rich PNA probe (Cy3; red) and mounted in Vectashield with DAPI. Maximum-intensity projections are presented for all color channels. The arrows point to close contacts between RAP1, telomeres, and ICP0* (readily visible in the merged image on the far right), suggesting that they are part of the same APB-like structure. (C) 3D reconstitution of the images in panel B. (D) Immuno-FISH on *S. granarius* metaphase chromosomes, combining antibodies to human RAP1 (green) and a telomeric PNA probe (Cy3; red); chromosomes are stained with DAPI. Bars, 10 μm.

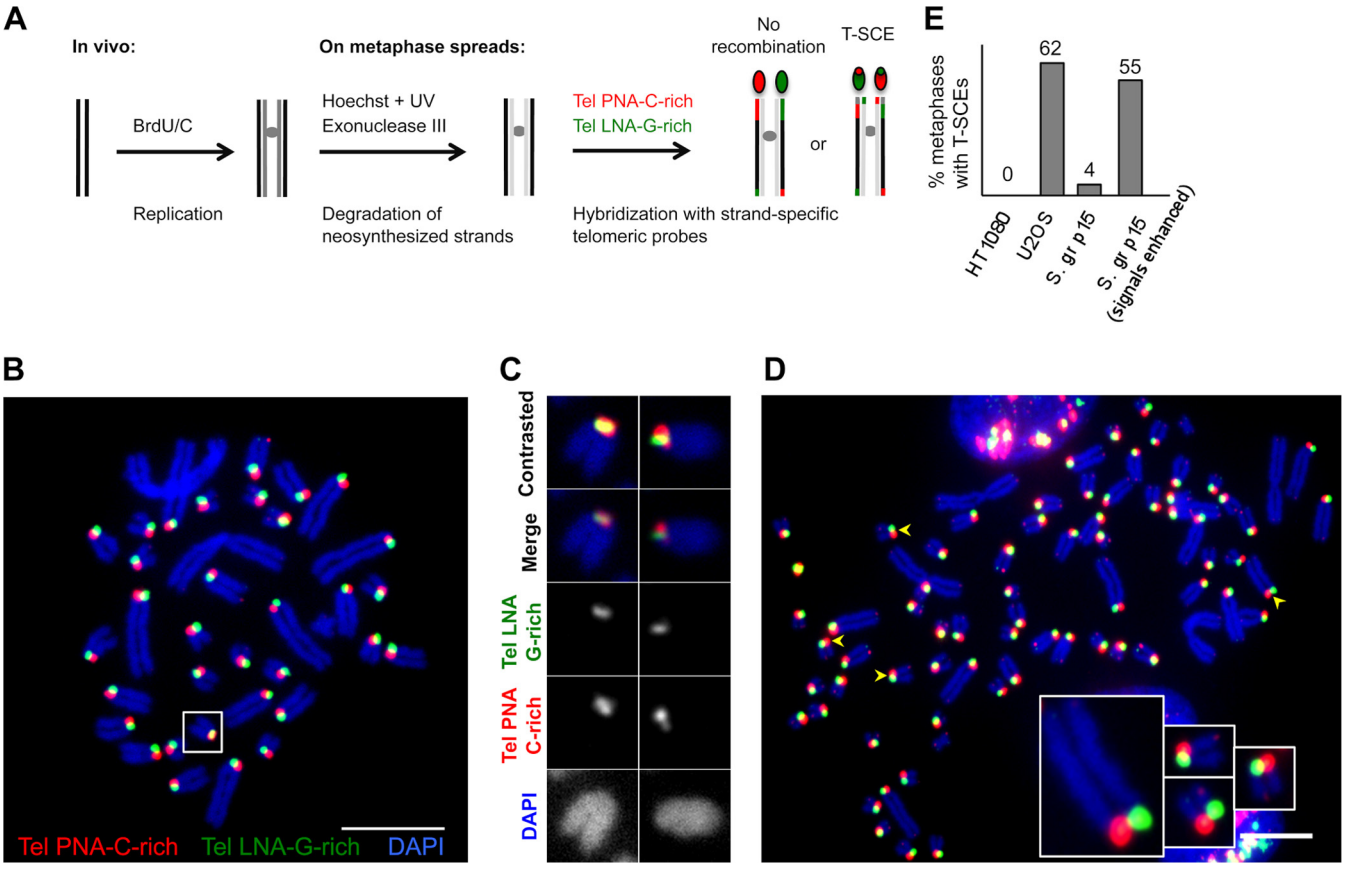

FIG 5 Recombination at telomeres in *S. granarius*. (A) CO-FISH approach to reveal T-SCEs. After the removal of newly synthesized strands, a C-rich probe will exclusively detect the parental G-rich strand (one-color CO-FISH). If an exchange has taken place after replication, two signals instead of one will be detected at the chromosome extremity. In two-color CO-FISH, strand-specific C-rich and G-rich telomeric probes are used, and T-SCEs are detected as mixed red-green signals. (B) CO-FISH using two strand-specific telomeric probes: TelPNA-C-rich-Cy3 (red) and Tel-LNA-G-rich-FAM (green). Chromosomes were counterstained with DAPI (blue). Only long telomeres present on short acrocentric arms were analyzed. Most extremities show one single green or red robust signal per chromatid. The box indicates a chromosome with mixed signals, indicating a T-SCE. Affected chromosomes varied from metaphase to metaphase. Quantifications of different experiments using one- or two-color CO-FISH are presented in panel E and Table 2. (C) Examples of T-SCEs detected in *S. granarius* early-passage fibroblasts (p15). (D) Signal enhancement allows the detection of potential highly asymmetric exchanges (very weak green signals colocalizing with the strong red signal, and vice versa [arrowheads]). Enlarged examples are presented. The segregated CO-FISH analysis presented in Fig. 6 indicates that such colocalizations correspond to bona fide T-SCEs. Bars, 10 μm. (E) Quantification of T-SCEs in *S. granarius* early-passage (S. gr p15) fibroblasts relative to U2OS/ALT and HT1080/TEL$^+$ human cancer cell lines (n = 30 metaphase spreads for each condition). The frequency of metaphase chromosomes carrying T-SCEs when only "robust" fluorescence signals are taken into account appears to be low in *S. granarius* fibroblasts. However, when T-SCEs are searched upon enhancement of signals, the frequency is much higher. The fact that these are bone fide T-SCEs was confirmed by segregated CO-FISH analysis (Fig. 6).

signal in interphase nuclei of *S. granarius*. However, we found that antibodies against human RAP1 revealed intranuclear foci that partially overlapped the telomeric signals (Fig. 4B and C). The fact that these antibodies recognized telomere-associated structures was further confirmed in IF experiments using metaphase chromosomes from *S. granarius*, since the anti-RAP1 antibodies yielded fluorescent spots that perfectly colocalized with telomere signals revealed by a PNA probe (Fig. 4D). In interphase nuclei, on the other hand, strong RAP1 foci were in close contact both with ICP0* and with telomere foci (Fig. 4B and C). Together, these observations strongly suggest that at least some of the telomere aggregates detected in *S. granarius* nuclei are in close contact with (or part of) NBs containing an ICP0* target, most likely the PML protein. Thus, such nuclear bodies display some similarity to the APBs found in human ALT cells (13).

***S. granarius* telomeres show active recombination.** We next looked for signs of telomere recombination in primary *S. granarius* fibroblasts by using the CO-FISH technique (Fig. 5A). Using this technique, it has been shown that telomere-sister chromatid exchanges (T-SCEs) are very rare or totally absent in human primary or immortal cells that do not use ALT for telomere elongation (7, 15). CO-FISH experiments using *S. granarius* fibroblasts, on the other hand, revealed the presence of T-SCEs (Fig. 5B to D and Table 2). The frequency of metaphase chromosomes carrying T-SCEs was not very high compared to that for the human cancer ALT cell line U2OS when only robust fluorescence signals were taken into account (Fig. 5E). However, when enhanced images were examined, T-SCEs could be observed at many chromosome extremities with both one-color (not shown) and two-color CO-FISH (Fig. 5D), thus suggesting that these reactions transferred limited material from one sister chromatid to the other. One major technical concern in CO-FISH experiments is the partial degradation of the newly synthesized strand by ExoIII (due to the partial incorporation of BrdU/C), which typically yields highly asymmetric doublets, very similar to what we observed in *S. granarius*. In an attempt to determine whether the high level of asym-

TABLE 2 Frequencies of T-SCEs in primary *S. granarius* fibroblast cells (passages 4 to 8)[a]

Culture type and expt no.	No. of metaphase spreads analyzed	No. of extremities with long telomeres	No. of metaphase spreads with:		% of metaphase spreads with T-SCEs (±SEM)
			1 T-SCE	>1 T-SCE	
Asynchronous					
1	86	2,738	40	5	52.3
2	90	2,870	43	7	55.6
3	70	2,216	37	4	58.6
Total	246	7,824	120	16	55.5 (±3.8)
Synchronous					
1	100	3,191	42	7	49.0
2	90	2,872	43	8	56.6
Total	190	6,063	85	15	52.3 (±4.8)

[a] T-SCEs in primary *S. granarius* fibroblasts were detected using one-color CO-FISH. Chromosome material was prepared from both asynchronous (three independent experiments) and synchronized (serum starvation; two independent experiments) cell cultures.

metric doublets corresponded to true exchanges or to a technical artifact, we examined cells after two rounds of replication in the presence of BrdU/C, a procedure we named segregated CO-FISH (Fig. 6). Chromosome segregation following the first mitosis will separate the sister chromatids bearing unsubstituted telomere strands, such that chromosomes in the second mitosis will show only one of the labels on one of the sister chromatids (Fig. 6A). In the absence of T-SCE, no signal should be detected on the other sister chromatid. If a T-SCE occurred before the first division, the sister chromatid carrying both unsubstituted G-rich and C-rich sequences would yield, during the second mitotic phase, a chromosome carrying a sister chromatid with unsubstituted G-rich sequences and another with unsubstituted C-rich sequences that will resist strand degradation and will be detected by the probes (Fig. 6B). Unsubstituted strands originating from partial BrdU/C incorporation during the first cell cycle will also yield a similar

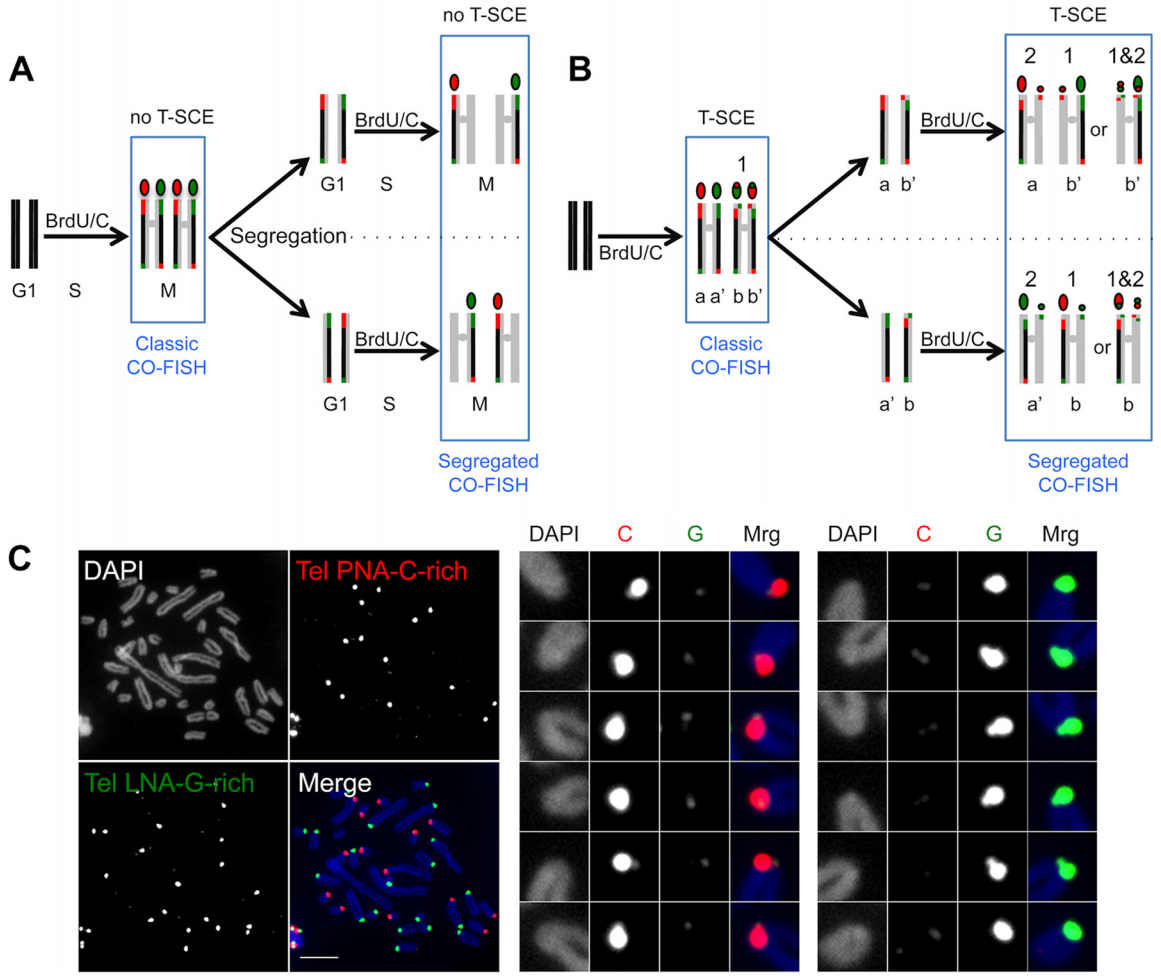

FIG 6 (A) BrdU/C incorporation during two cell cycles prior to the CO-FISH procedure, using strand-specific telomeric probes, results in segregation of the unsubstituted G- and C-rich strands into different chromosomes, such that during the second M phase, every chromosome extremity will be stained, after the CO-FISH procedure, with only one probe, either red (TelPNA-C-rich-Cy3) or green (TelLNA-G-rich-FAM). (B) If a T-SCE occurs during the first cell cycle, the two unsubstituted strands will cosegregate during the first mitosis and will be detected on different sister chromatids of the same chromosome during the second M phase. The CO-FISH procedure will then reveal one red and one green signal on the same chromosome extremity (marked 1). If a T-SCE occurs during the second cell cycle, this exchange will result in same-color doublets, either red or green (marked 2). However, if a second exchange affects an extremity that had already undergone T-SCE during the first cell cycle, doublets will be of both colors (marked 1&2). (C) Two-color segregated CO-FISH in *S. granarius*. Highly asymmetric two-color doublets are frequently detected in *S. granarius* fibroblasts (p15). Examples of such T-SCEs are enlarged and color decomposed on the right. The TelPNA-C-rich-Cy3 probe is more efficient than the TelLNA-G-rich-FAM probe for detecting small doublets. Chromosomes were counterstained with DAPI (blue). Bar, 10 μm.

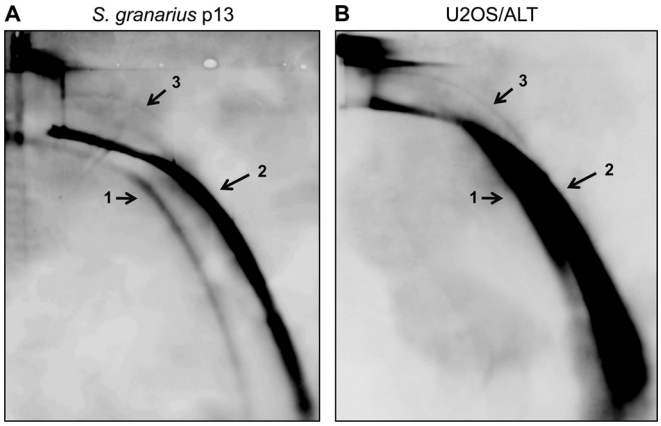

FIG 7 Telomeric circles are detected in primary *S. granarius* fibroblasts. Ten micrograms of genomic DNA from *S. granarius* early-passage (p13) fibroblasts (A) and 20 μg genomic DNA from the human ALT cancer cell line U2OS (B) were digested with MboI, separated by 2D gel electrophoresis, transferred onto N+ nylon membranes, and hybridized with a digoxigenin-labeled telomeric C-rich oligonucleotide. Arrow 1, single-stranded linear DNA; arrow 2, double-stranded linear DNA; arrow 3, circular DNA.

result, so this approach is unable to distinguish between bona fide T-SCEs and spurious signals. However, since cells were in contact with BrdU/C during the totality of the second cell cycle, partial incorporation during the second round of replication can be excluded, and therefore any presence of G-rich or C-rich doublets indicates a bona fide transfer of unsubstituted material to the other sister chromatid, i.e., a T-SCE. Using this approach, we revealed the presence of highly asymmetric doublets, very often colocalizing with small signals revealing the complementary strand (Fig. 6C). These observations are in agreement with the presence of a high level of T-SCEs affecting the long telomeres of *S. granarius*. In contrast, we did not detect exchanges on the short telomeres on the long arms (Fig. 5D and 6C), although the lack of sensitivity of CO-FISH and segregated CO-FISH may at least partially account for this failure.

Another feature related to the presence of a higher recombination activity at telomeres is the presence of T circles (30). Using a 2D gel electrophoresis approach to separate telomere restriction fragments (TRF) and extrachromosomal telomere material both by size and by shape, we detected T circles in both early- and late-passage *S. granarius* fibroblasts, further supporting the idea that telomere homologous recombination is derepressed in these cells (Fig. 7). We also detect extrachromosomal linear telomeric DNAs, another characteristic of ALT cells, most likely the by-products of telomere recombination and repair reactions (4). In contrast, C circles, one of the features most specifically related to ALT in human cells (31), were not detected in either early- or late-passage *S. granarius* fibroblasts (not shown).

***S. granarius* telomeres bear marks of DNA damage.** It was recently shown that ALT cells are also characterized by the presence of "uncapped" telomeres able to elicit a DNA damage response (DDR) that does not lead to chromosome-chromosome fusions (32). We therefore studied the status of telomere capping in primary fibroblasts of *S. granarius* by detecting the accumulation of γ-H2AX at telomeres (DDR^+) from metaphase chromosomes (Fig. 8). We confirmed by Western blot analysis that the available antibodies against γ-H2AX were specific in *S. granarius* cells, since they detected a signal of the molecular weight predicted for γ-H2AX, which was robustly induced by a short exposure to UVC rays (not shown).

We first performed a classic immuno-FISH experiment in which both telomeric DNA and γ-H2AX are detected simultaneously (one-step protocol) (32). In this experiment, strong γ-H2AX signals were almost exclusively associated with the long telomeres of acrocentric chromosomes, and, on average, 21% of chromosome ends were DDR^+ (Fig. 8A and Table 3). While most of these colocalizations between telomeric repeats and γ-H2AX signals were almost perfect, some ends showed γ-H2AX signals spread into subtelomeric positions (Fig. 8A and B). The meaning of these subtelomeric DDR signals remains unknown, but the possibility that they correspond to short (undetectable) interstitial telomere repeats cannot be excluded.

To exclude the possibility that γ-H2AX also frequently accumulated on short telomeres but the signals were destroyed during the hybridization phase of the one-step protocol, we undertook a two-step analysis in which anti-γ-H2AX staining was recorded before the hybridization step with the telomeric probe. In contrast to the immuno-FISH one-step experiment, the two-step approach allowed us to detect γ-H2AX signals on both the long and short telomeres (Fig. 8C). With this protocol, 44% of all chromosome ends showed γ-H2AX signals, and among those, two-thirds were on long telomeres (Table 3). We could distinguish two patterns of colocalization: associations with both chromatids (chromosome-type TIF) and association with only one chromatid (chromatid-type TIF) (Fig. 7D and Table 3). Distinguishing between the two provides information about the moment when the DNA damage occurred. Chromosome-type TIF suggest the presence of DNA damage prior to replication, while chromatid-type TIF are supposed to emerge after replication (33). This observation suggests that most spontaneous DDR at telomeres in early-passage *S. granarius* fibroblasts arises prereplicatively.

Interestingly, in interphase nuclei, γ-H2AX signals were frequently associated with large foci of telomeric DNA (Fig. 8E), suggesting that partially uncapped, DDR^+ telomeres associate to form APB-like structures.

Very short telomeres accumulate upon antitelomerase treatment of *S. granarius* fibroblasts. The presence of telomere recombination signatures in *S. granarius* fibroblasts opens the possibility that telomeres are maintained by ALT. However, telomeres on the long arms are kept homogenously short, even at advanced passages, suggesting that if ALT is at work in these cells, then these extremities are not the preferred substrates for interchromosome recombination. Thus, since it is likely that these telomeres are maintained by telomerase, we wondered whether inhibition of this enzymatic activity could trigger recombination at short telomeres, which should result in conspicuous length fluctuations measurable by Q-FISH (34). We treated *S. granarius* cells with BIBR1532, a nonnucleoside inhibitor of telomerase that is able to induce senescence in human cancer cells (35). After 2 months of treatment, we detected the accumulation of ultrashort telomeres on the long arms of treated cells (not shown). However, we could not detect any long arms carrying a long telomere. On the other hand, long telomeres, while remaining heterogeneous, also displayed shortening (not shown), indicating that telomerase contributed to the maintenance of telomere length on *S. granarius* acrocentric extremities.

***S. granarius* telomeres are transcribed.** It has been shown that telomeres in most organisms are not transcriptionally silent (36).

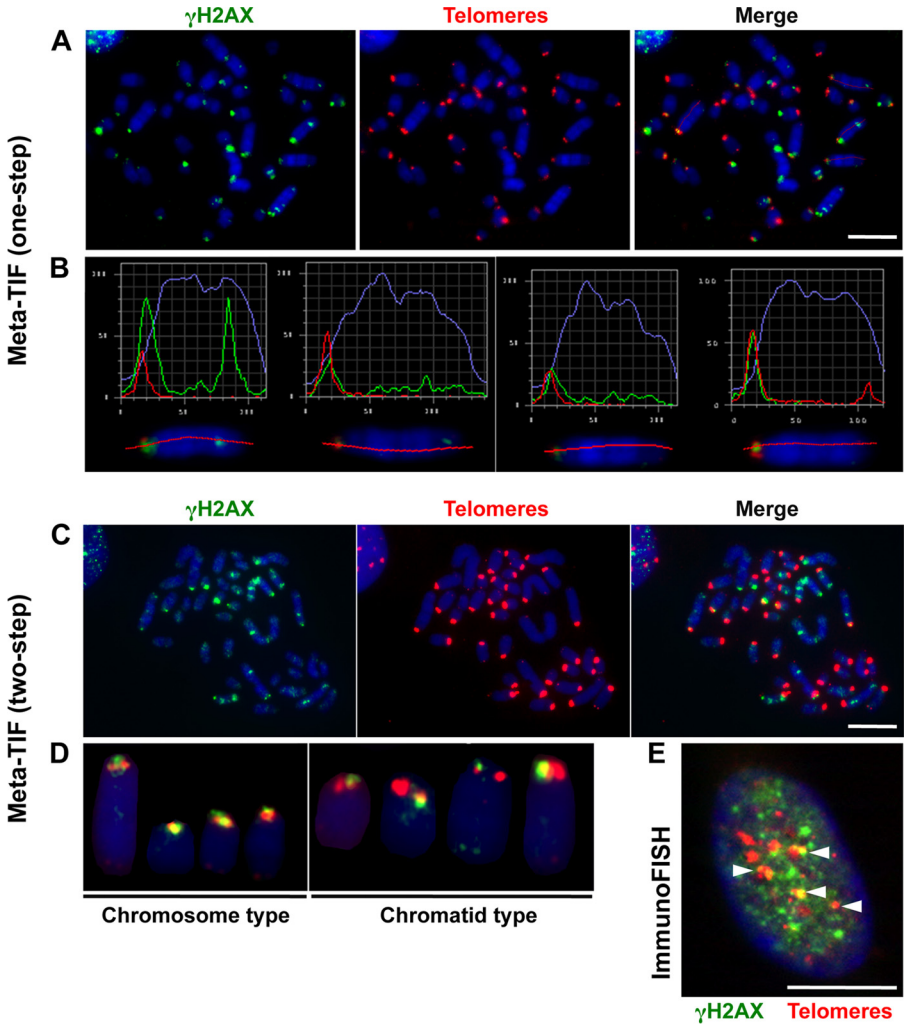

FIG 8 Spontaneous telomere dysfunction in primary *S. granarius* fibroblasts. (A) Meta-TIF analysis of *S. granarius* fibroblasts (one-step protocol). Metaphase chromosomes were first stained with anti-γH2AX antibodies (green) and subsequently stained with a telomeric PNA probe (red) for detection of telomere-induced foci (TIF). Chromosomes were counterstained with DAPI (blue). (B) Relative green and red fluorescence intensities of particular chromosomes from the metaphase spread shown in panel A, illustrating either perfect colocalization of red and green signals or the spread of green signals toward the interstitial region. (C) Meta-TIF analysis of *S. granarius* fibroblasts by a two-step protocol involving immunofluorescence assay with anti-γH2AX antibodies, with image acquisition (green; left panel), as well as hybridization with a telomeric PNA probe, with visualization (red; middle panel). The right panel show the merge of the two visualization steps. (D) Illustration of chromosome- and chromatid-type TIF detected in a two-step experiment. The images show staining with anti-γH2AX antibodies (green) and a telomeric PNA probe (red). A quantification of these experiments is presented in Table 3. (E) Detection of TIF in *S. granarius* interphase nucleus by a one-step protocol. The image shows staining with anti-γH2AX antibodies (green) and a telomeric PNA probe (red). Bars, 10 μm.

We explored whether this is the case for *S. granarius* telomeres. Indeed, RNA FISH using a C-rich telomeric probe showed RNase-sensitive telomeric foci on nondenatured metaphase preparations, indicating the accumulation of TERRA at *S. granarius* telomeres (Fig. 9A and B). Interestingly, the same experiment using a G-rich probe also showed accumulation of RNase-sensitive signals at telomeres, indicating that the C-rich strand was also transcribed. Both types of telomeric RNA were frequently detected as

TABLE 3 Frequencies of DDR$^+$ telomeres in primary *S. granarius* fibroblast cells (passages 3 to 7)[a]

Expt (*n*)	No. of metaphase spreads analyzed	No. of chromosomes analyzed	Avg no. of chromosomes per metaphase spread	Avg no. of DDR$^+$ telomeres per metaphase spread (±SEM)	
				Long telomeres	Short telomeres
One-step expt (2)	100	3,588	35.9	14.95 (±3.05)	NA
Two-step expt (1)	62	2,228	35.9	22 (±2.32), among which 16.3 (±4.5) were of the chromosome type	10 (±1.67), among which 7.3 (±1.8) were of the chromosome type

[a] The presence of a DNA damage response (DDR) at telomeres was assessed in early-passage *S. granarius* fibroblasts. Two different protocols were employed. The two-step protocol was more sensitive and also allowed the detection of DDR on short telomeres. Around 44% of all chromosome ends were positive for DDR, with a great majority being of the chromosome type (both sister chromatids are labeled). NA, not available (short telomeres were often undetectable under these experimental conditions).

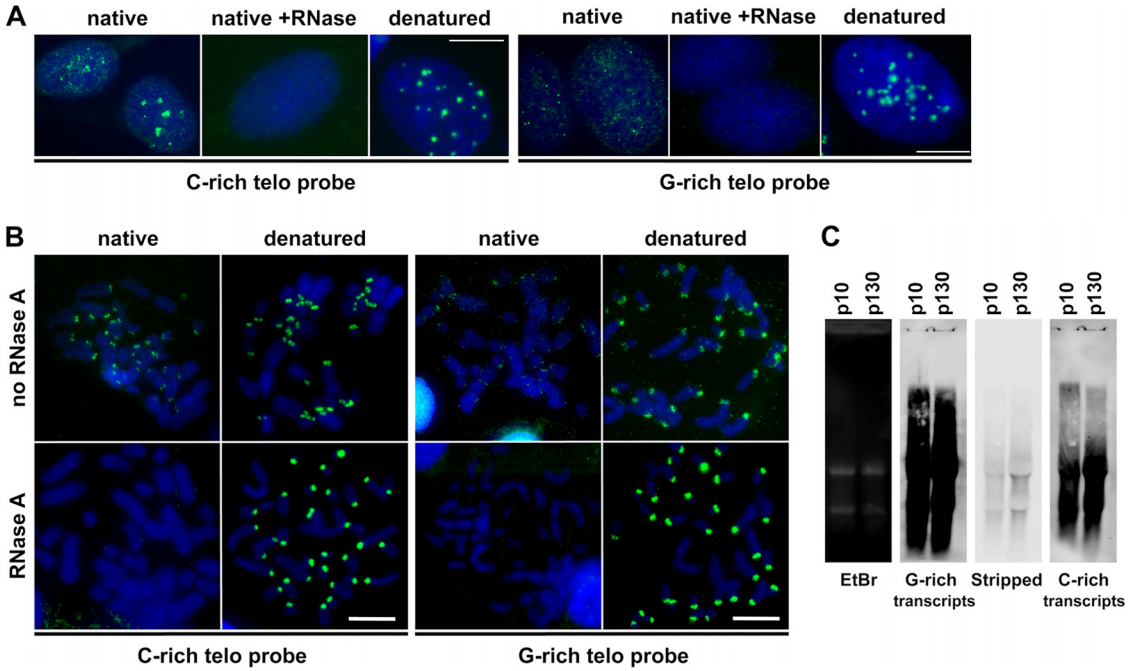

FIG 9 Both G-rich and C-rich telomere strands are expressed in *S. granarius* cells. (A) RNA FISH experiments with strand-specific probes on *S. granarius* interphase nuclei. The C-rich probe detected either the UUAGGG or TTAGGG sequence, and the G-rich probe detected either CCCUAA or CCCTAA, depending on whether the hybridization was done on native or denatured nuclei, respectively. Signals were visible with both probes under native conditions without RNase treatment, albeit at lower intensity when the probe was G-rich. The signal was completely lost when native preparations were treated with RNase. Both probes detected telomeres equally efficiently under denaturing conditions. Nuclei are stained with DAPI (blue). (B) Similar RNA FISH experiment on metaphase chromosome preparations obtained by cytospin centrifugation under native or denatured conditions and treated or not treated with RNase. Once again, the C-rich probe yielded stronger signals than the G-rich probe, only on native, RNase-untreated chromosomes. Bars, 10 μm. (C) Northern blot analysis of *S. granarius* telomeric RNA transcripts in cells at different passages (p). (Left) Visualization of total RNA in the gel by ethidium bromide (EtBr) staining before transfer onto a membrane. (Second panel) Hybridization with a C-rich telomere probe labeled with digoxigenin. (Third panel) Verification of the stripping efficiency. (Right) Hybridization with a G-rich probe labeled with digoxigenin.

multiple foci associated with the same chromosome extremity. Northern blot analysis confirmed the presence of both G-rich and C-rich RNA species in *S. granarius* early- and late-passage fibroblasts (Fig. 9C).

DISCUSSION

S. granarius has a particular telomere structure among mammals. Telomeric and rDNA (18S rDNA) repeats are found together, either interspersed or in tandem, on the short arms of all 32 acrocentric at chromosomes. It is worth noting that this is the only placental mammal in which a telomere structure composed of discontinuous telomere repeats interspersed with rDNA has been found (8). Our studies now indicate that at least some of these rDNA loci are transcribed. On the other hand, given the interspersed nature of *S. granarius* telomere repeats and their conserved strand specificity (as ascertained by CO-FISH analysis), it was possible that blocks of interstitial telomere repeats could be transcribed on both strands. Indeed, we detected the accumulation of transcripts containing either G-rich or C-rich sequences. In mammals, telomeric RNA strands containing G-rich telomeric repeats are transcribed from the subtelomeric region (17). In *Schizosaccharomyces pombe*, however, some proportion of telomeric RNAs are C-rich, suggesting that the C-rich strand is transcribed from promoter sites within the telomere repeats (36). It is therefore possible that the C-rich RNA species found in *S. granarius* are transcribed from promoters located not only in the interspersed nontelomeric sequences but also in the repeated telomere sequence itself.

Our studies indicate that *S. granarius* telomeres do not mediate replicative senescence. The presence of telomerase activity and signs of telomere recombination from the earliest passages of *S. granarius* fibroblasts, as well as the rather limited telomere shortening after numerous passages, together with the absence of gross structural chromosome rearrangements, indicate that telomere length is actively maintained and telomeres remain functional. Note that it has been suggested that oxidative stress is a major source of telomere damage in mammalian species with a small body size and whose cells do not use replicative senescence when cultured *in vitro* (8). This may very well be the case for *S. granarius* fibroblasts, which mostly present persistent prereplicative, chromosome-type telomere damage. It is also possible that DDR$^+$ telomeres in primary *S. granarius* fibroblasts are more related to the use of recombination-based mechanisms for telomere maintenance. Interestingly, *S. granarius* fibroblasts appear to be totally devoid of C circles, which are considered the most specific hallmark of ALT in human tumor cells (31). The origin of C circles remains unknown but may be related to replication-related processes, as they are triggered, along with all other ALT hallmarks, by suppression of the histone chaperone ASF1 (37). Alternatively, although C circles are highly specific, they may not be present in all ALT tumors, especially tumors in which telomerase activity is also detected (38). Furthermore, it has been suggested that expression of telomerase suppresses the presence of C circles without affecting other ALT hallmarks (38). Thus, the absence of C circles in *S.*

granarius fibroblasts may be explained by the presence of telomerase activity, which was found to also target long telomeres.

Indeed, in human cells, the reactivation of telomerase activity in ALT cells most often leads to the maintenance of telomere length by both mechanisms, indicating that they are compatible (39–41). The natural coexistence of both mechanisms may occur *in vivo*, as recently indicated by the discovery of ALT-like intertelomeric recombination in mouse somatic tissues (42). Strikingly, although the recombination-based telomere elongation mechanism may in principle act on every chromosome end, we found that in *S. granarius* cells, the shortest telomeres, always associated with the long arms of acrocentric chromosomes, were kept homogeneously short even after more than 100 passages. This observation suggests that these extremities are excluded from recombination and, rather, maintained by telomerase. While telomerase may preferentially work on short telomeres (16, 43), it is not clear why the relatively short telomeres of *S. granarius* are prevented from participating in recombination reactions. Even when telomerase activity was (at least partially) inhibited and very short telomeres accumulated at those extremities, we did not detect abrupt elongation events, as expected if ALT takes over telomere length maintenance (34). One possibility is that recombination is initiated on flanking interspersed sequences that are otherwise completely absent on the short telomeres. Another, nonexclusive possibility is that short telomeres are never recruited to recombination centers, likely represented here by the APB-like structures formed by the long telomeres.

The origin of the unusual *S. granarius* chromosome structure is not clear, and we can only speculate on whether or not there is any relationship between the emergence/maintenance of such a structure and the presence of rampant telomere recombination in this organism. It has been proposed that the ancestor for all sibling species of the *Sorex araneus* group, including *S. granarius*, had a pattern of telomeric and rDNA distribution similar to the modern pattern of *S. araneus* race Cordon, that is, extremities bearing a few rDNA loci located near telomeres (11). During the evolution of the *S. granarius* karyotype, the fission of metacentric chromosomes and the telomerization of the newly created short arms could have provoked an overall reorganization of chromosome ends. The shuffling of large telomere-repeat-containing blocks, through inter- and intrachromosomal homologous recombination involving the adjacent rDNA loci, but perhaps with the contribution of break-induced replication mechanisms that are thought be at play in ALT and that can copy large domains of DNA until the tip of the chromosome arm is reached (44–47), could lead to the duplication and amplification of both telomeric and ribosomal DNAs on the short arms of all acrocentric chromosomes in *S. granarius*. The recombinogenic telomeres present in this organism nowadays may constitute a mechanistic vestige of such duplication events in evolution. Duplication, translocation, and amplification of subtelomeric sequences are quite frequent phenomena during karyotype evolution, as illustrated by the spectacular evolution of the heterochromatic caps in the great apes and the evolution of juxtatelomeric sequences in humans (48–51). Interestingly, large domains of telomere repeats are absent from these duplicated, amplified sequences most of the time, suggesting either that they do not often participate in (or, perhaps, do suppress) such events or that telomere repeats are eliminated most of the time in the course of evolution. In striking contrast, large telomere-like repeat sequences are associated with a subset of subtelomeric heterochromatic caps in gorilla chromosomes (52). However, these are not canonical telomere repeats, suggesting that a certain degree of degeneration was necessary to tolerate large telomeric repeat domains at subtelomeric positions (52). In *S. granarius*, telomere tandem repeats are theoretically mostly canonical (that is, efficiently recognized by PNA probes), suggesting that sequence conservation at interstitial locations was important in this case. The CO-FISH data suggest that sister chromatid exchanges most often involve short stretches of telomere repeats and, therefore, that such limited exchanges may be akin to gene conversion events (53), which may have contributed to the sequence conservation in *S. granarius* large telomeres. How crossovers leading to exchange of large segments are most of the time prevented remains unknown, but the presence of interspersed rDNA might influence recombination processes between telomere repeats. Moreover, rDNA interspersion may have helped to stabilize the large stretches of telomere repeats on the long arms of *S. granarius*, thus conferring an advantage to the whole structure. Conversely, interspersed telomere repeats may have an impact on rDNA biology, perhaps through replication processes, which could be facilitated by the presence of shelterin-like components (54). Finally, the *S. granarius* acrocentric extremities may represent an extreme example of the impact that telomere physiology has on nucleolar stability and structural integrity of acrocentric chromosomes, a relationship that has just started to be unveiled in human cells (55). More work is necessary to address these questions, provided that specific tools for research in *S. granarius* are developed.

ACKNOWLEDGMENTS

This work was partly supported by a budgetary project of the Institute of Cytology and Genetics of SB RAS VI.53.1.4, Project RAS "Living nature: modern status and problems of development" 30-32, and by the CNRS, through the PIC program. C.L.N. was a recipient of a fellowship from the Institut Curie. R.M.P. obtained a Ph.D. fellowship from the Institut Curie and Association pour la Recherche contre le Cancer. The Telomere & Cancer Laboratory is supported by the Ligue Nationale contre le Cancer.

REFERENCES

1. **Pfeiffer V, Lingner J.** 2013. Replication of telomeres and the regulation of telomerase. Cold Spring Harb. Perspect. Biol. **5:**a010405. http://dx.doi.org/10.1101/cshperspect.a010405.
2. **Tumpel S, Rudolph KL.** 2012. The role of telomere shortening in somatic stem cells and tissue aging: lessons from telomerase model systems. Ann. N. Y. Acad. Sci. **1266:**28–39. http://dx.doi.org/10.1111/j.1749-6632.2012.06547.x.
3. **Hug N, Lingner J.** 2006. Telomere length homeostasis. Chromosoma **115:**413–425. http://dx.doi.org/10.1007/s00412-006-0067-3.
4. **Pickett HA, Cesare AJ, Johnston RL, Neumann AA, Reddel RR.** 2009. Control of telomere length by a trimming mechanism that involves generation of t-circles. EMBO J. **28:**799–809. http://dx.doi.org/10.1038/emboj.2009.42.
5. **Griffith JD, Comeau L, Rosenfield S, Stansel RM, Bianchi A, Moss H, de Lange T.** 1999. Mammalian telomeres end in a large duplex loop. Cell **97:**503–514. http://dx.doi.org/10.1016/S0092-8674(00)80760-6.
6. **Wang RC, Smogorzewska A, de Lange T.** 2004. Homologous recombination generates T-loop-sized deletions at human telomeres. Cell **119:**355–368. http://dx.doi.org/10.1016/j.cell.2004.10.011.
7. **Cesare AJ, Reddel RR.** 2010. Alternative lengthening of telomeres: models, mechanisms and implications. Nat. Rev. Genet. **11:**319–330. http://dx.doi.org/10.1038/nrg2763.
8. **Gomes NM, Ryder OA, Houck ML, Charter SJ, Walker W, Forsyth NR, Austad SN, Venditti C, Pagel M, Shay JW, Wright WE.** 2011. Comparative biology of mammalian telomeres: hypotheses on ancestral states and the roles of telomeres in longevity determination. Aging Cell **10:**761–768. http://dx.doi.org/10.1111/j.1474-9726.2011.00718.x.
9. **Wyttenbach A, Borodin P, Hausser J.** 1998. Meiotic drive favors Robertsonian metacentric chromosomes in the common shrew (Sorex ara-

neus, Insectivora, Mammalia). Cytogenet. Cell Genet. **83:**199–206. http://dx.doi.org/10.1159/000015178.
10. **Zhdanova NS, Karamisheva TV, Minina J, Astakhova NM, Lansdorp P, Kammori M, Rubtsov NB, Searle JB.** 2005. Unusual distribution pattern of telomeric repeats in the shrews Sorex araneus and Sorex granarius. Chromosome Res. **13:**617–625. http://dx.doi.org/10.1007/s10577-005-0988-3.
11. **Zhdanova NS, Minina JM, Karamisheva TV, Draskovic I, Rubtsov NB, Londono-Vallejo JA.** 2007. The very long telomeres in Sorex granarius (Soricidae, Eulipothyphla) contain ribosomal DNA. Chromosome Res. **15:**881–890. http://dx.doi.org/10.1007/s10577-007-1170-x.
12. **Zhdanova NS, Rogozina Iu I, Minina Iu M, Borodin PM, Rubtsov NB.** 2009. Telomeric DNA allocation in chromosomes of common shrew Sorex araneus, Eulipotyphla. Tsitologiia **51:**577–584.
13. **Draskovic I, Arnoult N, Steiner V, Bacchetti S, Lomonte P, Londono-Vallejo A.** 2009. Probing PML body function in ALT cells reveals spatiotemporal requirements for telomere recombination. Proc. Natl. Acad. Sci. U. S. A. **106:**15726–15731. http://dx.doi.org/10.1073/pnas.0907689106.
14. **Everett RD, Earnshaw WC, Findlay J, Lomonte P.** 1999. Specific destruction of kinetochore protein CENP-C and disruption of cell division by herpes simplex virus immediate-early protein Vmw110. EMBO J. **18:**1526–1538. http://dx.doi.org/10.1093/emboj/18.6.1526.
15. **Londoño-Vallejo JA, Der-Sarkissian H, Cazes L, Bacchetti S, Reddel R.** 2004. Alternative lengthening of telomeres is characterized by high rates of inter-telomeric exchange. Cancer Res. **64:**2324–2327. http://dx.doi.org/10.1158/0008-5472.CAN-03-4035.
16. **Londono-Vallejo JA, DerSarkissian H, Cazes L, Thomas G.** 2001. Differences in telomere length between homologous chromosomes in humans. Nucleic Acids Res. **29:**3164–3171. http://dx.doi.org/10.1093/nar/29.15.3164.
17. **Azzalin CM, Reichenbach P, Khoriauli L, Giulotto E, Lingner J.** 2007. Telomeric repeat containing RNA and RNA surveillance factors at mammalian chromosome ends. Science **318:**798–801. http://dx.doi.org/10.1126/science.1147182.
18. **Ijdo JW, Wells RA, Baldini A, Reeders ST.** 1991. Improved telomere detection using a telomere repeat probe (TTAGGG)n generated by PCR. Nucleic Acids Res. **19:**4780. http://dx.doi.org/10.1093/nar/19.17.4780.
19. **Arnoult N, Shin-Ya K, Londono-Vallejo JA.** 2008. Studying telomere replication by Q-CO-FISH: the effect of telomestatin, a potent G-quadruplex ligand. Cytogenet. Genome Res. **122:**229–236. http://dx.doi.org/10.1159/000167808.
20. **Kim NW, Piatyszek MA, Prowse KR, Harley CB, West MD, Ho PL, Coviello GM, Wright WE, Weinrich SL, Shay JW.** 1994. Specific association of human telomerase activity with immortal cells and cancer. Science **266:**2011–2015. http://dx.doi.org/10.1126/science.7605428.
21. **Wege H, Chui MS, Le HT, Tran JM, Zern MA.** 2003. SYBR Green real-time telomeric repeat amplification protocol for the rapid quantification of telomerase activity. Nucleic Acids Res. **31:**E3-3. http://dx.doi.org/10.1093/nar/gng033.
22. **Grummt I.** 2003. Life on a planet of its own: regulation of RNA polymerase I transcription in the nucleolus. Genes Dev. **17:**1691–1702. http://dx.doi.org/10.1101/gad.1098503R.
23. **Klein J, Grummt I.** 1999. Cell cycle-dependent regulation of RNA polymerase I transcription: the nucleolar transcription factor UBF is inactive in mitosis and early G1. Proc. Natl. Acad. Sci. U. S. A. **96:**6096–6101. http://dx.doi.org/10.1073/pnas.96.11.6096.
24. **Draskovic I, Londono-Vallejo A.** 2013. Telomere recombination and alternative telomere lengthening mechanisms. Front. Biosci. **18:**1–20. http://dx.doi.org/10.2741/4084.
25. **Murnane JP, Sabatier L, Marder BA, Morgan WF.** 1994. Telomere dynamics in an immortal human cell line. EMBO J. **13:**4953–4962.
26. **Yeager TR, Neumann AA, Englezou A, Huschtscha LI, Noble JR, Reddel RR.** 1999. Telomerase-negative immortalized human cells contain a novel type of promyelocytic leukemia (PML) body. Cancer Res. **59:**4175–4179.
27. **Rubtsov IB, Karamysheva TV, Minina Iu M, Zhdanova NS.** 2008. 3D organization of interphase fibroblast nuclei in two closely related shrew species, Sorex granarius and S. araneus, differed by the structure of chromosome termini. Tsitologiia **50:**430–438.
28. **Lomonte P, Morency E.** 2007. Centromeric protein CENP-B proteasomal degradation induced by the viral protein ICP0. FEBS Lett. **581:**658–662. http://dx.doi.org/10.1016/j.febslet.2007.01.027.
29. **Torok D, Ching RW, Bazett-Jones DP.** 2009. PML nuclear bodies as sites of epigenetic regulation. Front. Biosci. (Landmark Ed.) **14:**1325–1336.
30. **Cesare AJ, Griffith JD.** 2004. Telomeric DNA in ALT cells is characterized by free telomeric circles and heterogeneous T-loops. Mol. Cell. Biol. **24:**9948–9957. http://dx.doi.org/10.1128/MCB.24.22.9948-9957.2004.
31. **Henson JD, Cao Y, Huschtscha LI, Chang AC, Au AY, Pickett HA, Reddel RR.** 2009. DNA C-circles are specific and quantifiable markers of alternative-lengthening-of-telomeres activity. Nat. Biotechnol. **27:**1181–1185. http://dx.doi.org/10.1038/nbt.1587.
32. **Cesare AJ, Kaul Z, Cohen SB, Napier CE, Pickett HA, Neumann AA, Reddel RR.** 2009. Spontaneous occurrence of telomeric DNA damage response in the absence of chromosome fusions. Nat. Struct. Mol. Biol. **16:**1244–1251. http://dx.doi.org/10.1038/nsmb.1725.
33. **Kaul Z, Cesare AJ, Huschtscha LI, Neumann AA, Reddel RR.** 2011. Five dysfunctional telomeres predict onset of senescence in human cells. EMBO Rep **13:**52–59. http://dx.doi.org/10.1038/embor.2011.227.
34. **Morrish TA, Greider CW.** 2009. Short telomeres initiate telomere recombination in primary and tumor cells. PLoS Genet. **5:**e1000357. http://dx.doi.org/10.1371/journal.pgen.1000357.
35. **Pascolo E, Wenz C, Lingner J, Hauel N, Priepke H, Kauffmann I, Garin-Chesa P, Rettig WJ, Damm K, Schnapp A.** 2002. Mechanism of human telomerase inhibition by BIBR1532, a synthetic, non-nucleosidic drug candidate. J. Biol. Chem. **277:**15566–15572. http://dx.doi.org/10.1074/jbc.M201266200.
36. **Bah A, Wischnewski H, Shchepachev V, Azzalin CM.** 2012. The telomeric transcriptome of Schizosaccharomyces pombe. Nucleic Acids Res. **40:**2995–3005. http://dx.doi.org/10.1093/nar/gkr1153.
37. **O'Sullivan RJ, Arnoult N, Lackner DH, Oganesian L, Haggblom C, Corpet A, Almouzni G, Karlseder J.** 2014. Rapid induction of alternative lengthening of telomeres by depletion of the histone chaperone ASF1. Nat. Struct. Mol. Biol. **21:**167–174. http://dx.doi.org/10.1038/nsmb.2754.
38. **Plantinga MJ, Pascarelli KM, Merkel AS, Lazar AJ, von Mehren M, Lev D, Broccoli D.** 2013. Telomerase suppresses formation of ALT-associated single-stranded telomeric C-circles. Mol. Cancer Res. **11:**557–567. http://dx.doi.org/10.1158/1541-7786.MCR-13-0013.
39. **Cerone MA, Londoño-Vallejo JA, Bacchetti S.** 2001. Telomere maintenance by telomerase and by recombination can coexist in human cells. Hum. Mol. Genet. **10:**1945–1952. http://dx.doi.org/10.1093/hmg/10.18.1945.
40. **Grobelny JV, Kulp-McEliece M, Broccoli D.** 2001. Effects of reconstitution of telomerase activity on telomere maintenance by the alternative lengthening of telomeres (ALT) pathway. Hum. Mol. Genet. **10:**1953–1961. http://dx.doi.org/10.1093/hmg/10.18.1953.
41. **Perrem K, Colgin LM, Neumann AA, Yeager TR, Reddel RR.** 2001. Coexistence of alternative lengthening of telomeres and telomerase in hTERT-transfected GM847 cells. Mol. Cell. Biol. **21:**3862–3875. http://dx.doi.org/10.1128/MCB.21.12.3862-3875.2001.
42. **Neumann AA, Watson CM, Noble JR, Pickett HA, Tam PP, Reddel RR.** 2013. Alternative lengthening of telomeres in normal mammalian somatic cells. Genes Dev. **27:**18–23. http://dx.doi.org/10.1101/gad.205062.112.
43. **Ouellette MM, Liao M, Herbert BS, Johnson M, Holt SE, Liss HS, Shay JW, Wright WE.** 2000. Subsenescent telomere lengths in fibroblasts immortalized by limiting amounts of telomerase. J. Biol. Chem. **275:**10072–10076. http://dx.doi.org/10.1074/jbc.275.14.10072.
44. **Costantino L, Sotiriou SK, Rantala JK, Magin S, Mladenov E, Helleday T, Haber JE, Iliakis G, Kallioniemi OP, Halazonetis TD.** 2014. Break-induced replication repair of damaged forks induces genomic duplications in human cells. Science **343:**88–91. http://dx.doi.org/10.1126/science.1243211.
45. **Lydeard JR, Jain S, Yamaguchi M, Haber JE.** 2007. Break-induced replication and telomerase-independent telomere maintenance require Pol32. Nature **448:**820–823. http://dx.doi.org/10.1038/nature06047.
46. **McEachern MJ, Haber JE.** 2006. Break-induced replication and recombinational telomere elongation in yeast. Annu. Rev. Biochem. **75:**111–135. http://dx.doi.org/10.1146/annurev.biochem.74.082803.133234.
47. **Saini N, Ramakrishnan S, Elango R, Ayyar S, Zhang Y, Deem A, Ira G, Haber JE, Lobachev KS, Malkova A.** 2013. Migrating bubble during break-induced replication drives conservative DNA synthesis. Nature **502:**389–392. http://dx.doi.org/10.1038/nature12584.
48. **Der-Sarkissian H, Vergnaud G, Borde YM, Thomas G, Londono-Vallejo JA.** 2002. Segmental polymorphisms in the proterminal regions of a subset of human chromosomes. Genome Res. **12:**1673–1678. http://dx.doi.org/10.1101/gr.322802.
49. **Mefford HC, Trask BJ.** 2002. The complex structure and dynamic evolution of human subtelomeres. Nat. Rev. Genet. **3:**91–102. http://dx.doi.org/10.1038/nrg727.

50. **Ventura M, Catacchio CR, Alkan C, Marques-Bonet T, Sajjadian S, Graves TA, Hormozdiari F, Navarro A, Malig M, Baker C, Lee C, Turner EH, Chen L, Kidd JM, Archidiacono N, Shendure J, Wilson RK, Eichler EE.** 2011. Gorilla genome structural variation reveals evolutionary parallelisms with chimpanzee. Genome Res. **21:**1640–1649. http://dx.doi.org/10.1101/gr.124461.111.
51. **Ventura M, Catacchio CR, Sajjadian S, Vives L, Sudmant PH, Marques-Bonet T, Graves TA, Wilson RK, Eichler EE.** 2012. The evolution of African great ape subtelomeric heterochromatin and the fusion of human chromosome 2. Genome Res. **22:**1036–1049. http://dx.doi.org/10.1101/gr.136556.111.
52. **Novo CL, Arnoult N, Liu W-Y, Castro Vega LJ, Gibaud A, Dutrillaux B, Bacchetti S, Londono-Vallejo A.** 2013. The heterochromatic chromosome caps in great apes impact telomere metabolism. Nucleic Acids Res. **41:**4792–4801. http://dx.doi.org/10.1093/nar/gkt169.
53. **Helleday T.** 2003. Pathways for mitotic homologous recombination in mammalian cells. Mutat. Res. **532:**103–115. http://dx.doi.org/10.1016/j.mrfmmm.2003.08.013.
54. **Sfeir A, Kosiyatrakul ST, Hockemeyer D, MacRae SL, Karlseder J, Schildkraut CL, de Lange T.** 2009. Mammalian telomeres resemble fragile sites and require TRF1 for efficient replication. Cell **138:**90–103. http://dx.doi.org/10.1016/j.cell.2009.06.021.
55. **Stimpson KM, Sullivan LL, Kuo ME, Sullivan BA.** 2014. Nucleolar organization, ribosomal DNA array stability, and acrocentric chromosome integrity are linked to telomere function. PLoS One **9:**e92432. http://dx.doi.org/10.1371/journal.pone.0092432.